SLAC-PUB-15047

BABAR BAD Note 2416 Version 021

Study of high-multiplicity 3-prong and 5-prong τ decays at BABAR

J. P. Lees, V. Poireau, and V. Tisserand
Laboratoire d'Annecy-le-Vieux de Physique des Particules (LAPP), Université de Savoie, CNRS/IN2P3, F-74941 Annecy-Le-Vieux, France

J. Garra Tico and E. Grauges
Universitat de Barcelona, Facultat de Fisica, Departament ECM, E-08028 Barcelona, Spain

A. Palano[ab]
INFN Sezione di Bari[a]; Dipartimento di Fisica, Università di Bari[b], I-70126 Bari, Italy

G. Eigen and B. Stugu
University of Bergen, Institute of Physics, N-5007 Bergen, Norway

D. N. Brown, L. T. Kerth, Yu. G. Kolomensky, and G. Lynch
Lawrence Berkeley National Laboratory and University of California, Berkeley, California 94720, USA

H. Koch and T. Schroeder
Ruhr Universität Bochum, Institut für Experimentalphysik 1, D-44780 Bochum, Germany

D. J. Asgeirsson, C. Hearty, T. S. Mattison, J. A. McKenna, and R. Y. So
University of British Columbia, Vancouver, British Columbia, Canada V6T 1Z1

A. Khan
Brunel University, Uxbridge, Middlesex UB8 3PH, United Kingdom

V. E. Blinov, A. R. Buzykaev, V. P. Druzhinin, V. B. Golubev, E. A. Kravchenko, A. P. Onuchin, S. I. Serednyakov, Yu. I. Skovpen, E. P. Solodov, K. Yu. Todyshev, and A. N. Yushkov
Budker Institute of Nuclear Physics, Novosibirsk 630090, Russia

M. Bondioli, D. Kirkby, A. J. Lankford, and M. Mandelkern
University of California at Irvine, Irvine, California 92697, USA

H. Atmacan, J. W. Gary, F. Liu, O. Long, and G. M. Vitug
University of California at Riverside, Riverside, California 92521, USA

C. Campagnari, T. M. Hong, D. Kovalskyi, J. D. Richman, and C. A. West
University of California at Santa Barbara, Santa Barbara, California 93106, USA

A. M. Eisner, J. Kroseberg, W. S. Lockman, A. J. Martinez, B. A. Schumm, and A. Seiden
University of California at Santa Cruz, Institute for Particle Physics, Santa Cruz, California 95064, USA

D. S. Chao, C. H. Cheng, B. Echenard, K. T. Flood, D. G. Hitlin, P. Ongmongkolkul, F. C. Porter, and A. Y. Rakitin
California Institute of Technology, Pasadena, California 91125, USA

R. Andreassen, Z. Huard, B. T. Meadows, M. D. Sokoloff, and L. Sun
University of Cincinnati, Cincinnati, Ohio 45221, USA

P. C. Bloom, W. T. Ford, A. Gaz, U. Nauenberg, J. G. Smith, and S. R. Wagner
University of Colorado, Boulder, Colorado 80309, USA

R. Ayad* and W. H. Toki
Colorado State University, Fort Collins, Colorado 80523, USA

B. Spaan

Work supported in part by US Department of Energy contract DE-AC02-76SF00515.

SLAC National Accelerator Laboratory, Menlo Park, CA 94025

Technische Universität Dortmund, Fakultät Physik, D-44221 Dortmund, Germany

K. R. Schubert and R. Schwierz
Technische Universität Dresden, Institut für Kern- und Teilchenphysik, D-01062 Dresden, Germany

D. Bernard and M. Verderi
Laboratoire Leprince-Ringuet, Ecole Polytechnique, CNRS/IN2P3, F-91128 Palaiseau, France

P. J. Clark and S. Playfer
University of Edinburgh, Edinburgh EH9 3JZ, United Kingdom

D. Bettoni[a], C. Bozzi[a], R. Calabrese[ab], G. Cibinetto[ab], E. Fioravanti[ab], I. Garzia[ab], E. Luppi[ab], M. Munerato[ab], L. Piemontese[a], and V. Santoro[a]
INFN Sezione di Ferrara[a]; Dipartimento di Fisica, Università di Ferrara[b], I-44100 Ferrara, Italy

R. Baldini-Ferroli, A. Calcaterra, R. de Sangro, G. Finocchiaro, P. Patteri, I. M. Peruzzi,[†] M. Piccolo, M. Rama, and A. Zallo
INFN Laboratori Nazionali di Frascati, I-00044 Frascati, Italy

R. Contri[ab], E. Guido[ab], M. Lo Vetere[ab], M. R. Monge[ab], S. Passaggio[a], C. Patrignani[ab], and E. Robutti[a]
INFN Sezione di Genova[a]; Dipartimento di Fisica, Università di Genova[b], I-16146 Genova, Italy

B. Bhuyan and V. Prasad
Indian Institute of Technology Guwahati, Guwahati, Assam, 781 039, India

C. L. Lee and M. Morii
Harvard University, Cambridge, Massachusetts 02138, USA

A. J. Edwards
Harvey Mudd College, Claremont, California 91711

A. Adametz and U. Uwer
Universität Heidelberg, Physikalisches Institut, Philosophenweg 12, D-69120 Heidelberg, Germany

H. M. Lacker and T. Lueck
Humboldt-Universität zu Berlin, Institut für Physik, Newtonstr. 15, D-12489 Berlin, Germany

P. D. Dauncey
Imperial College London, London, SW7 2AZ, United Kingdom

U. Mallik
University of Iowa, Iowa City, Iowa 52242, USA

C. Chen, J. Cochran, W. T. Meyer, S. Prell, and A. E. Rubin
Iowa State University, Ames, Iowa 50011-3160, USA

A. V. Gritsan and Z. J. Guo
Johns Hopkins University, Baltimore, Maryland 21218, USA

N. Arnaud, M. Davier, D. Derkach, G. Grosdidier, F. Le Diberder, A. M. Lutz, B. Malaescu, P. Roudeau, M. H. Schune, A. Stocchi, and G. Wormser
Laboratoire de l'Accélérateur Linéaire, IN2P3/CNRS et Université Paris-Sud 11, Centre Scientifique d'Orsay, B. P. 34, F-91898 Orsay Cedex, France

D. J. Lange and D. M. Wright
Lawrence Livermore National Laboratory, Livermore, California 94550, USA

C. A. Chavez, J. P. Coleman, J. R. Fry, E. Gabathuler, D. E. Hutchcroft, D. J. Payne, and C. Touramanis

University of Liverpool, Liverpool L69 7ZE, United Kingdom

A. J. Bevan, F. Di Lodovico, R. Sacco, and M. Sigamani
Queen Mary, University of London, London, E1 4NS, United Kingdom

G. Cowan
University of London, Royal Holloway and Bedford New College, Egham, Surrey TW20 0EX, United Kingdom

D. N. Brown and C. L. Davis
University of Louisville, Louisville, Kentucky 40292, USA

A. G. Denig, M. Fritsch, W. Gradl, K. Griessinger, A. Hafner, and E. Prencipe
Johannes Gutenberg-Universität Mainz, Institut für Kernphysik, D-55099 Mainz, Germany

R. J. Barlow,[‡] G. Jackson, and G. D. Lafferty
University of Manchester, Manchester M13 9PL, United Kingdom

E. Behn, R. Cenci, B. Hamilton, A. Jawahery, and D. A. Roberts
University of Maryland, College Park, Maryland 20742, USA

C. Dallapiccola
University of Massachusetts, Amherst, Massachusetts 01003, USA

R. Cowan, D. Dujmic, and G. Sciolla
Massachusetts Institute of Technology, Laboratory for Nuclear Science, Cambridge, Massachusetts 02139, USA

R. Cheaib, D. Lindemann, P. M. Patel, and S. H. Robertson
McGill University, Montréal, Québec, Canada H3A 2T8

P. Biassoni[ab], N. Neri[a], F. Palombo[ab], and S. Stracka[ab]
INFN Sezione di Milano[a]; Dipartimento di Fisica, Università di Milano[b], I-20133 Milano, Italy

L. Cremaldi, R. Godang,[§] R. Kroeger, P. Sonnek, and D. J. Summers
University of Mississippi, University, Mississippi 38677, USA

X. Nguyen, M. Simard, and P. Taras
Université de Montréal, Physique des Particules, Montréal, Québec, Canada H3C 3J7

G. De Nardo[ab], D. Monorchio[ab], G. Onorato[ab], and C. Sciacca[ab]
INFN Sezione di Napoli[a]; Dipartimento di Scienze Fisiche,
Università di Napoli Federico II[b], I-80126 Napoli, Italy

M. Martinelli and G. Raven
NIKHEF, National Institute for Nuclear Physics and High Energy Physics, NL-1009 DB Amsterdam, The Netherlands

C. P. Jessop, J. M. LoSecco, and W. F. Wang
University of Notre Dame, Notre Dame, Indiana 46556, USA

K. Honscheid and R. Kass
Ohio State University, Columbus, Ohio 43210, USA

J. Brau, R. Frey, N. B. Sinev, D. Strom, and E. Torrence
University of Oregon, Eugene, Oregon 97403, USA

E. Feltresi[ab], N. Gagliardi[ab], M. Margoni[ab], M. Morandin[a],
M. Posocco[a], M. Rotondo[a], G. Simi[a], F. Simonetto[ab], and R. Stroili[ab]
INFN Sezione di Padova[a]; Dipartimento di Fisica, Università di Padova[b], I-35131 Padova, Italy

S. Akar, E. Ben-Haim, M. Bomben, G. R. Bonneaud, H. Briand, G. Calderini, J. Chauveau, O. Hamon, Ph. Leruste, G. Marchiori, J. Ocariz, and S. Sitt
Laboratoire de Physique Nucléaire et de Hautes Energies, IN2P3/CNRS, Université Pierre et Marie Curie-Paris6, Université Denis Diderot-Paris7, F-75252 Paris, France

M. Biasini[ab], E. Manoni[ab], S. Pacetti[ab], and A. Rossi[ab]
INFN Sezione di Perugia[a]; Dipartimento di Fisica, Università di Perugia[b], I-06100 Perugia, Italy

C. Angelini[ab], G. Batignani[ab], S. Bettarini[ab], M. Carpinelli[ab],¶ G. Casarosa[ab], A. Cervelli[ab], F. Forti[ab], M. A. Giorgi[ab], A. Lusiani[ac], B. Oberhof[ab], E. Paoloni[ab], A. Perez[a], G. Rizzo[ab], and J. J. Walsh[a]
INFN Sezione di Pisa[a]; Dipartimento di Fisica, Università di Pisa[b]; Scuola Normale Superiore di Pisa[c], I-56127 Pisa, Italy

D. Lopes Pegna, J. Olsen, A. J. S. Smith, and A. V. Telnov
Princeton University, Princeton, New Jersey 08544, USA

F. Anulli[a], R. Faccini[ab], F. Ferrarotto[a], F. Ferroni[ab], M. Gaspero[ab], L. Li Gioi[a], M. A. Mazzoni[a], and G. Piredda[a]
INFN Sezione di Roma[a]; Dipartimento di Fisica, Università di Roma La Sapienza[b], I-00185 Roma, Italy

C. Bünger, O. Grünberg, T. Hartmann, T. Leddig, H. Schröder, C. Voss, and R. Waldi
Universität Rostock, D-18051 Rostock, Germany

T. Adye, E. O. Olaiya, and F. F. Wilson
Rutherford Appleton Laboratory, Chilton, Didcot, Oxon, OX11 0QX, United Kingdom

S. Emery, G. Hamel de Monchenault, G. Vasseur, and Ch. Yèche
CEA, Irfu, SPP, Centre de Saclay, F-91191 Gif-sur-Yvette, France

D. Aston, D. J. Bard, R. Bartoldus, J. F. Benitez, C. Cartaro, M. R. Convery, J. Dorfan, G. P. Dubois-Felsmann, W. Dunwoodie, M. Ebert, R. C. Field, M. Franco Sevilla, B. G. Fulsom, A. M. Gabareen, M. T. Graham, P. Grenier, C. Hast, W. R. Innes, M. H. Kelsey, P. Kim, M. L. Kocian, D. W. G. S. Leith, P. Lewis, B. Lindquist, S. Luitz, V. Luth, H. L. Lynch, D. B. MacFarlane, D. R. Muller, H. Neal, S. Nelson, M. Perl, T. Pulliam, B. N. Ratcliff, A. Roodman, A. A. Salnikov, R. H. Schindler, A. Snyder, D. Su, M. K. Sullivan, J. Va'vra, A. P. Wagner, W. J. Wisniewski, M. Wittgen, D. H. Wright, H. W. Wulsin, C. C. Young, and V. Ziegler
SLAC National Accelerator Laboratory, Stanford, California 94309 USA

W. Park, M. V. Purohit, R. M. White, and J. R. Wilson
University of South Carolina, Columbia, South Carolina 29208, USA

A. Randle-Conde and S. J. Sekula
Southern Methodist University, Dallas, Texas 75275, USA

M. Bellis, P. R. Burchat, and T. S. Miyashita
Stanford University, Stanford, California 94305-4060, USA

M. S. Alam and J. A. Ernst
State University of New York, Albany, New York 12222, USA

R. Gorodeisky, N. Guttman, D. R. Peimer, and A. Soffer
Tel Aviv University, School of Physics and Astronomy, Tel Aviv, 69978, Israel

P. Lund and S. M. Spanier
University of Tennessee, Knoxville, Tennessee 37996, USA

J. L. Ritchie, A. M. Ruland, R. F. Schwitters, and B. C. Wray
University of Texas at Austin, Austin, Texas 78712, USA

J. M. Izen and X. C. Lou
University of Texas at Dallas, Richardson, Texas 75083, USA

F. Bianchi[ab], D. Gamba[ab], and S. Zambito[ab]
INFN Sezione di Torino[a]; Dipartimento di Fisica Sperimentale, Università di Torino[b], I-10125 Torino, Italy

L. Lanceri[ab] and L. Vitale[ab]
INFN Sezione di Trieste[a]; Dipartimento di Fisica, Università di Trieste[b], I-34127 Trieste, Italy

F. Martinez-Vidal and A. Oyanguren
IFIC, Universitat de Valencia-CSIC, E-46071 Valencia, Spain

H. Ahmed, J. Albert, Sw. Banerjee, F. U. Bernlochner, H. H. F. Choi, G. J. King, R. Kowalewski, M. J. Lewczuk, I. M. Nugent, J. M. Roney, R. J. Sobie, and N. Tasneem
University of Victoria, Victoria, British Columbia, Canada V8W 3P6

T. J. Gershon, P. F. Harrison, T. E. Latham, and E. M. T. Puccio
Department of Physics, University of Warwick, Coventry CV4 7AL, United Kingdom

H. R. Band, S. Dasu, Y. Pan, R. Prepost, and S. L. Wu
University of Wisconsin, Madison, Wisconsin 53706, USA

(Dated: May 31, 2012)

Abstract

We present measurements of the branching fractions of 3-prong and 5-prong τ decay modes using a sample of 430 million τ lepton pairs, corresponding to an integrated luminosity of 468 fb^{-1}, collected with the *BABAR* detector at the PEP-II asymmetric energy e^+e^- storage rings. The $\tau^- \to (3\pi)^-\eta\nu_\tau$, $\tau^- \to (3\pi)^-\omega\nu_\tau$ and $\tau^- \to \pi^- f_1(1285)\nu_\tau$ branching fractions are presented as well as a new limit on the branching fraction of the isospin-forbidden, second-class current $\tau^- \to \pi^-\eta'(958)\nu_\tau$ decay. We find no evidence for charged kaons in these decay modes and place the first upper limits on their branching fractions.

PACS numbers: 13.35.Dx, 14.60.Fg

I. INTRODUCTION

The *BABAR* Collaboration has studied 3-prong and 5-prong τ decay modes where "prong" refers to the number of charged hadrons (π^- or K^-) in the final state (for example, see [1], [2]). The study of these decays was motivated by a search for the second-class current $\tau^- \to \pi^-\eta'(958)\nu_\tau$, which is forbidden if isospin is conserved. The selection criteria developed to search for second-class current decays are also able to identify many other rare or previously unobserved τ decay modes. As a result, we have used the large *BABAR* τ data sample to make a comprehensive study of these high-multiplicity decay modes.

We present measurements of the $\tau^- \to (3\pi)^-\eta\nu_\tau$, $\tau^- \to (3\pi)^-\omega\nu_\tau$ and $\tau^- \to \pi^- f_1\nu_\tau$ branching fractions. Here and throughout this paper, charge conjugation is implied. We use the primary decay modes of the η, ω and f_1 mesons: $\eta \to \gamma\gamma$, $\eta \to \pi^+\pi^-\pi^0$, $\eta \to 3\pi^0$, $\omega \to \pi^-\pi^+\pi^0$, $f_1 \to 2\pi^+2\pi^-$ and $f_1 \to \pi^+\pi^-\eta$ (note that the f_1 meson studied in the work is the $f_1(1258)$). No other narrow resonances are observed. We find that these modes with narrow resonances cannot account for all of the observed decays. We measure the branching fraction of the "non-resonant" decays although these decays may involve a broad underlying resonance. In addition to the new limit on the branching fraction of the second-class current $\tau^- \to \pi^-\eta'(958)\nu_\tau$ decay, we present the first limits on the allowed (first-class current) $\tau^- \to K^-\eta'(958)\nu_\tau$ and $\tau^- \to \pi^-\eta'(958)\pi^0\nu_\tau$ decays using the $\eta' \to \pi^-\pi^+\eta$ decay mode. Finally, we present the first limits on the branching fractions of 5-prong decay modes in which one or more of the charged hadrons is a charged kaon.

This analysis is based on data recorded by the *BABAR* detector at the PEP-II asymmetric-energy e^+e^- storage rings operated at the laboratory known as the SLAC National Accelerator Laboratory. The data sample corresponds to an integrated luminosity ($\mathcal{L}$) of 468 fb^{-1} recorded at center-of-mass (CM) energies of 10.58 GeV and 10.54 GeV. This data sample contains approximately 430 million τ lepton pairs using the measured $e^+e^- \to \tau^+\tau^-$ cross-section of $\sigma_{\tau^+\tau^-} = (0.919 \pm 0.003)$ nb [3].

The *BABAR* detector is described in detail in Ref. [4]. Charged particle momenta are measured with a five-layer double-sided silicon vertex tracker and a 40-layer drift

*Now at the University of Tabuk, Tabuk 71491, Saudi Arabia chamber inside a 1.5 T superconducting solenoidal magnet. A detector of internally reflected Cerenkov light provides charged π/K separation [5] . A calorimeter consisting of CsI(Tl) crystals measures the energy of electromagnetic showers, and an instrumented magnetic flux return is used to identify muons.

The background contamination and selection efficiencies are determined using Monte Carlo simulation. The τ-pair production is simulated with the KK2F Monte Carlo event generator [6]. The τ decays, continuum $q\overline{q}$ events, and final-state radiative effects are modeled with Tauola [7], JETSET [8], and Photos [9], respectively. Dedicated samples of $\tau^+\tau^-$ events are created using Tauola or EvtGen [10] where one of the τ leptons can decay to any mode and the other τ decays to a specific final state. The detector response is simulated with GEANT4 [11]. All Monte Carlo simulation events are passed through a full simulation of the *BABAR* detector and are reconstructed in the same way as the data.

II. EVENT SELECTION

The τ pair is produced back-to-back in the e^+e^- CM frame. As a result, the decay products of the two τ leptons can be separated from each other by dividing the event into two hemispheres – the "signal" hemisphere and the "tag" hemisphere – using the event thrust axis [12] which is calculated using all charged particle and photon candidates ("neutral clusters") in the event.

We select events where one hemisphere (tag) contains exactly one track and the opposite hemisphere (signal) contains exactly three or five tracks with total charge opposite to the tag hemisphere. The event is rejected if any pair of oppositely charged tracks is consistent with being a photon conversion. The component of the momentum transverse to the beam axis for each of the tracks must be greater than 0.1 GeV/c in the laboratory frame. All tracks are required to have the point of closest approach to the interaction region less than 1.5 cm in the plane transverse to the e^- beam axis and less than 2.5 cm in the direction of the e^- beam axis. This eliminates K^0_S mesons that decay to $\pi^+\pi^-$ at points distant from the e^+e^- collision point.

To reduce backgrounds from non-τ pair events, we require that the momentum of the charged particle in the tag hemisphere be less than 4 GeV/c in the CM frame and be identified as an electron (e-tag) or a muon (μ-tag). The $q\overline{q}$ background is suppressed by requiring there be at most one electromagnetic calorimeter cluster in the tag hemisphere that is not associated to the track and has an energy less than 1 GeV. Additional suppression of the background events is achieved by requiring the magnitude of the event thrust to be between 0.92 and 0.99.

We reject events in which the invariant mass (M) of the charged particles, and the π^0 and η candidates, all in the signal hemisphere, is greater than 1.8 GeV/c^2. Neutral pion and eta candidates are reconstructed from two neutral candidates, each with energy greater than 30 MeV in the laboratory frame; the invariant mass of the π^0 (η) is required to be between 0.115(0.35) and 0.150 (0.70) GeV/c^2. Neutral pion candidates are reconstructed first in the signal hemisphere; the candidate with an invariant mass closest to the nominal π^0 mass is selected. The residual neutral clusters are used to search for the $\eta \rightarrow \gamma\gamma$ candidates. If there are more than two neutral clusters, we select the candidate whose invariant mass is closest to the nominal mass [17].

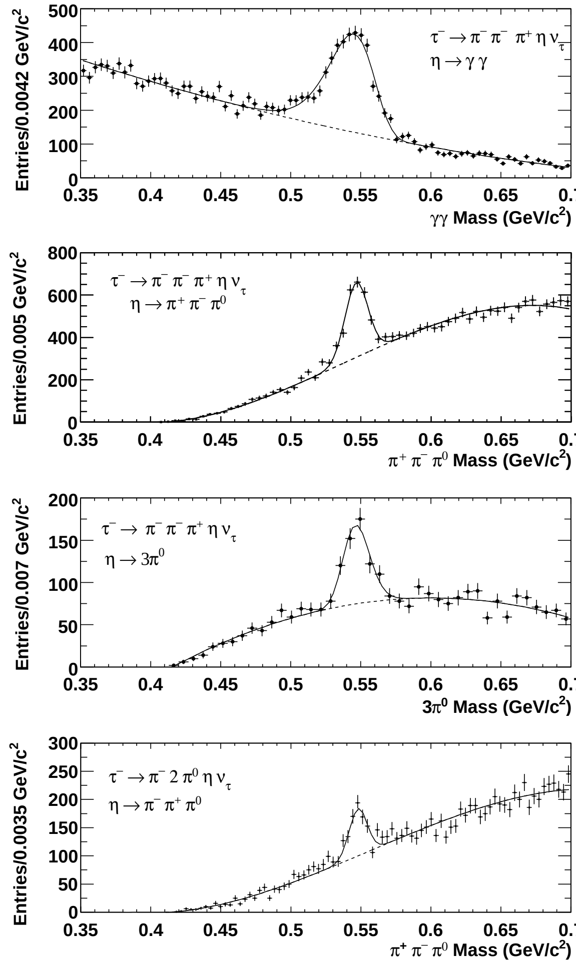

FIG. 1: The $\gamma\gamma$, $\pi^+\pi^-\pi^0$ and $3\pi^0$ invariant mass distributions for $\tau^- \rightarrow \pi^-\pi^-\pi^+\eta\nu_\tau$ decays, and the $\pi^+\pi^-\pi^0$ invariant mass distribution for $\tau^- \rightarrow \pi^- 2\pi^0\eta\nu_\tau$ decays in the data sample after all selection criteria are applied. The solid lines represent the simultaneous fit to the η peak and background. The dashed lines show the extrapolation of the background function under the η peak.

The branching fractions are calculated using $\mathcal{B} = N_X/(2N\varepsilon)$ where N_X is the number of candidates after background subtraction. The number of τ pairs, N, is determined from the product of the integrated luminosity times the $e^+e^- \rightarrow \tau^+\tau^-$ cross-section and the

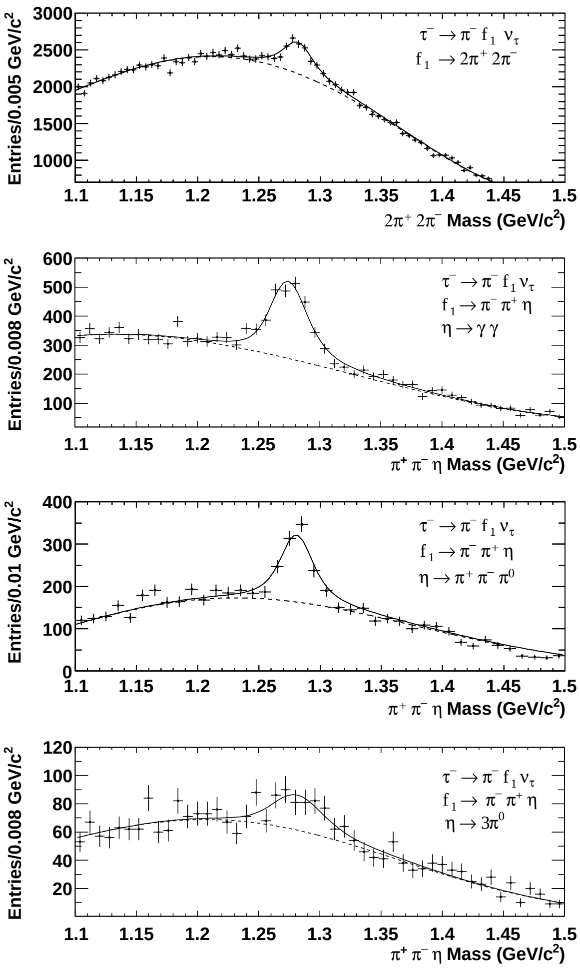

FIG. 2: The $2\pi^+$ $2\pi^-$ (top plot) and $\pi^+\pi^-\eta$ invariant mass distributions for $\tau^- \to \pi^-\pi^-\pi^+\eta\nu_\tau$ decays in the data sample after all selection criteria are applied. The lower three plots are for the $\eta \to \gamma\gamma$, $\eta \to \pi^+\pi^-\pi^0$ and $\eta \to 3\pi^0$ decays. The solid lines represent the simultaneous fit to the $f_1(1285)$ peak and background. The dashed lines show the extrapolation of the background function under the f_1 peak.

uncertainty is estimated to be 1%. The selection efficiencies (ϵ) are determined from the signal Monte Carlo samples. The uncertainty on the selection efficiencies includes 0.5% per track on the track reconstruction efficiency, as well as particle identification (PID) selection uncertainties. From studies conducted on real and simulated events, the uncertainty on the charged particle identification selectors are estimated to be 1% for electrons, 2.5% for muons, 0.5% for pions, and 1.8% for kaons. The combined electron and muon particle identification uncertainty is estimated to be 1.6% based on the composition of the event samples. The uncertainty on the $\pi^0 \to \gamma\gamma$ and $\eta \to \gamma\gamma$ reconstruction efficiency is estimated to be 3% per candidate.

III. RESULTS

We present measurements of τ decays to a system with η, f_1 and ω resonances in Sections A, B, and C, respectively. Decays with these resonances cannot account for all three or five prong τ decays and we present measurements of the tau branching fraction through non-resonant modes detailed in Section D. Finally, in Sections E and F we present searches for τ decays containing an η' (958) meson or up to two charged kaons.

A. $\tau^- \to (3\pi)^-\eta\nu_\tau$

The $\tau^- \to \pi^-\pi^-\pi^+\eta\nu_\tau$ mode is studied in the $\eta \to \gamma\gamma$, $\eta \to \pi^+\pi^-\pi^0$ and $\eta \to 3\pi^0$ final states while the $\tau^- \to \pi^- 2\pi^0\eta\nu_\tau$ mode is studied in the $\eta \to \pi^+\pi^-\pi^0$ final state.

The number of decays is determined by fitting the η mass peak in the $\gamma\gamma$, $\pi^+\pi^-\pi^0$ and $3\pi^0$ invariant mass distributions (see Fig. 1). The fit uses a Novosibirsk function (Gaussian distribution with a tail parameter) [13] for the η and a polynomial function for the background.

The Monte Carlo simulation predicts that some of the events in the η peak are from $e^+e^- \to q\overline{q}$. Control samples, obtained by reversing the requirement on the invariant mass of the observed decay products ($M > 1.8\,\mathrm{GeV}/c^2$), are used to verify the background estimate. If the ratio of data to Monte Carlo events in the control sample is found to be different than unity, then the number of background events is corrected by the ratio, and the statistical uncertainty of the ratio is included in the background systematic uncertainty. This method of verifying the $q\overline{q}$ background is used for all decays and will not be mentioned in the later sections.

The reconstruction efficiencies are determined from fits to the signal Monte Carlo samples. The $\tau^- \to \pi^- 2\pi^0\eta\nu_\tau$ sample is generated using a phase space model for the final state particles. The $\tau^- \to \pi^-\pi^-\pi^+\eta\nu_\tau$ sample is composed of $\tau^- \to \pi^- f_1\nu_\tau$ ($f_1 \to \pi^+\pi^-\eta$) decays and decays without an intermediate resonance. The $\tau^- \to \pi^-\pi^-\pi^+\eta\nu_\tau$ (excluding f_1) and $\tau^- \to \pi^- f_1\nu_\tau$ efficiencies are the same for $\eta \to \pi^+\pi^-\pi^0$ and $\eta \to 3\pi^0$, whereas a slight difference is observed for $\eta \to \gamma\gamma$. The difference is added to the selection efficiency systematic uncertainty for the $\tau^- \to \pi^-\pi^-\pi^+\eta\nu_\tau$ decay via the $\eta \to \gamma\gamma$ mode.

The three determinations of the $\tau^- \to \pi^-\pi^-\pi^+\eta\nu_\tau$ branching fraction are found to be in good agreement (see Table I); the average branching fraction (inclusive of $\tau^- \to \pi^- f_1\nu_\tau$) is

$$\mathcal{B}(\tau^- \to \pi^-\pi^-\pi^+\eta\nu_\tau) = (2.25 \pm 0.07 \pm 0.12) \times 10^{-4}.$$

Hereinafter, when two uncertainties are quoted, the first is statistical and the second is systematic. The branching fraction shown is the weighted average obtained by combining the statistical and systematic uncertainties in quadrature, accounting for correlations in the systematic uncertainties.

TABLE I: Results and branching fractions of $\tau^- \to (3\pi)^- \eta\nu_\tau$ decays

	$\tau^- \to \pi^-\pi^-\pi^+\eta\nu_\tau$ $\eta \to \gamma\gamma$	$\tau^- \to \pi^-\pi^-\pi^+\eta\nu_\tau$ $\eta \to \pi^+\pi^-\pi^0$	$\tau^- \to \pi^-\pi^-\pi^+\eta\nu_\tau$ $\eta \to 3\pi^0$	$\tau^- \to \pi^-2\pi^0\eta\nu_\tau$ $\eta \to \pi^+\pi^-\pi^0$
Branching fraction (10^{-4})	$2.10 \pm 0.09 \pm 0.13$	$2.37 \pm 0.12 \pm 0.18$	$2.65 \pm 0.28 \pm 0.27$	$2.01 \pm 0.34 \pm 0.24$
Data events	2887 ± 103	1440 ± 68	315 ± 34	381 ± 45
χ^2/NDF	107/76	60/52	31/34	95/75
Selection efficiency	$(3.83 \pm 0.11)\%$	$(2.97 \pm 0.02)\%$	$(0.42 \pm 0.01)\%$	$(0.75 \pm 0.02)\%$
Background events	131 ± 29	65 ± 38	< 1	83 ± 12
Systematic uncertainties (%)				
Tracking efficiency	2.7	3.8	2.7	2.7
π^0 and η PID	3.0	3.0	9.0	9.0
Pion PID	1.5	2.5	1.5	1.5
Lepton-tag PID	1.6	1.6	1.6	1.6
$\mathcal{L}\ \sigma_{\tau^+\tau^-}$	1.0	1.0	1.0	1.0
Selection efficiency	3.0	4.0	2.8	2.7
Background Modeling	1.0	2.8	1.6	4.0
$\mathcal{B}(\eta \to \gamma\gamma)$	1.0	-	-	-
$\mathcal{B}(\eta \to \pi^+\pi^-\pi^0)$	-	1.8	-	1.8
$\mathcal{B}(\eta \to 3\pi^0)$	-	-	0.9	-
Total (%)	6.3	7.4	10	11

The $\tau^- \to \pi^-2\pi^0\eta\nu_\tau$ branching fraction is found to be

$$\mathcal{B}(\tau^- \to \pi^-2\pi^0\eta\nu_\tau) = (2.0 \pm 0.3 \pm 0.2) \times 10^{-4}.$$

Naively, we expect the ratio of the $\tau^- \to \pi^-\pi^-\pi^+\eta\nu_\tau$ to $\tau^- \to \pi^-2\pi^0\eta\nu_\tau$ branching fractions to be 2 : 1 if the decay is dominated by the $\tau^- \to \pi^- f_1\nu_\tau$ decay mode (based on the f_1 branching fractions [17]).

The previous measurement of the $\tau^- \to \pi^-\pi^-\pi^+\eta\nu_\tau$ via $\eta \to \gamma\gamma$ branching fraction $(1.60 \pm 0.05 \pm 0.11) \times 10^{-4}$ [1] is superseded by this measurement.

The $\tau^- \to \pi^-\pi^-\pi^+\eta\nu_\tau$ and $\tau^- \to \pi^-2\pi^0\eta\nu_\tau$ branching fractions are in good agreement with the results from the CLEO Collaboration of $(2.3 \pm 0.5) \times 10^{-4}$ and $(1.5 \pm 0.5) \times 10^{-4}$, respectively [14]. Li predicts a larger $\tau^- \to \pi^-\pi^-\pi^+\eta\nu_\tau$ branching fraction of 2.93×10^{-4} [15].

B. $\tau^- \to \pi^- f_1\nu_\tau$

The branching fraction of $\tau^- \to \pi^- f_1\nu_\tau$ and the mass of the f_1 meson are measured using the $f_1 \to 2\pi^+2\pi^-$ and $f_1 \to \pi^+\pi^-\eta$ decay modes, where the $f_1 \to \pi^+\pi^-\eta$ decay is reconstructed using $\eta \to \gamma\gamma$, $\eta \to \pi^+\pi^-\pi^0$ and $\eta \to 3\pi^0$. The criteria used to select the $\tau^- \to \pi^- f_1\nu_\tau$ decays for the branching fraction measurement were described earlier. We modified the selection for the mass measurement, dropping the requirement that the track in the tag hemisphere be a lepton and the restriction on the number of neutral clusters in the tag hemisphere, to increase the size of the event sample.

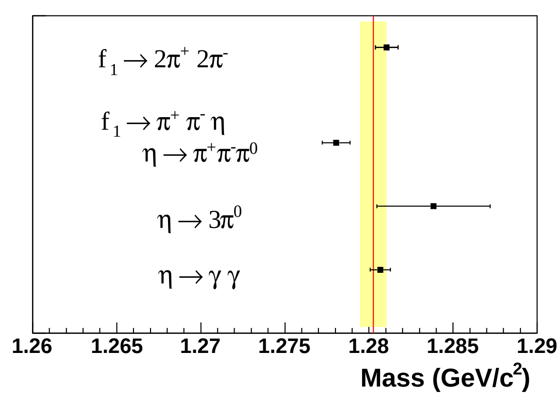

FIG. 3: Compilation of measurements of the f_1 invariant mass. The values shown do not include the global mass correction obtained from fits to other resonances. The solid line is the weighted average value and the shaded area is the one-standard-deviation region.

The number of $\tau^- \to \pi^- f_1\nu_\tau$ candidates is determined by fitting the f_1 peak in the $2\pi^+2\pi^-$ and $\pi^+\pi^-\eta$ invariant mass distributions (see Fig. 2). The f_1 lineshape is expected to be a Breit-Wigner distribution, modified by the limited phase space. Previous results show that the $f_1 \to a_0^-\pi^+$ $(a_0^-(980) \to \pi^-\eta)$ appears to account for all the $f_1 \to \pi^+\pi^-\eta$ decays [16]. The mass of the $\pi - a_0(980)$

TABLE II: Results and branching fractions of $\tau^- \to \pi^- f_1 \nu_\tau$ decays

	$f_1 \to 2\pi^+ 2\pi^-$	$f_1 \to \pi^+\pi^-\eta$ $\eta \to \gamma\gamma$	$f_1 \to \pi^+\pi^-\eta$ $\eta \to \pi^+\pi^-\pi^0$	$f_1 \to \pi^+\pi^-\eta$ $\eta \to 3\pi^0$
Branching fractions (10^{-4})				
$\mathcal{B}(\tau^- \to \pi^- f_1 \nu_\tau)$	$4.73 \pm 0.28 \pm 0.45$			
$\mathcal{B}(\tau^- \to \pi^- f_1 \nu_\tau)\mathcal{B}(f_1 \to \pi^-\pi^+\eta)$		$1.25 \pm 0.08 \pm 0.07$	$1.26 \pm 0.11 \pm 0.08$	$1.33 \pm 0.39 \pm 0.14$
Data events	3722 ± 222	1605 ± 94	731 ± 62	197 ± 59
χ^2/NDF	77/62	50/43	61/55	39/43
Selection efficiency	$(8.3 \pm 0.1)\%$	$(3.75 \pm 0.04)\%$	$(2.97 \pm 0.05)\%$	$(0.53 \pm 0.02)\%$
Systematic uncertainties (%)				
Tracking efficiency	3.8	2.7	3.8	2.7
π^0 and η PID	-	3.0	3.0	9.0
Pion PID	2.5	1.5	2.5	1.5
Lepton-tag PID	1.6	1.6	1.6	1.6
$\mathcal{L}\ \sigma_{\tau^+\tau^-}$	1.0	1.0	1.0	1.0
Selection efficiency	0.6	1.1	1.6	4.1
Fit model	5.0	2.7	-	-
$\mathcal{B}(f_1 \to 2\pi^+2\pi^-)$	6.4	-	-	-
$\mathcal{B}(\eta \to \gamma\gamma)$	-	0.7	-	-
$\mathcal{B}(\eta \to \pi^+\pi^-\pi^0)$	-	-	1.2	-
$\mathcal{B}(\eta \to 3\pi^0)$	-	-	-	0.9
Total (%)	9.5	5.6	6.1	11

system and the τ mass provide a lower and upper limit, respectively, on the f_1 lineshape. We use the four-vectors of the charged pion and $a_0(980)$ from the EvtGen generator to determine the f_1 lineshape and find it to be a close approximation of the Breit-Wigner expectation. The f_1 peak is fit using this lineshape convolved with a Gaussian distribution to take into account the effects of the detector resolution. The results of the fits are presented in Table II. There is no evidence for peaking background from $q\bar{q}$ events or other τ decays. This is confirmed by selecting events above the τ mass and seeing no f_1 candidates in either the data and Monte Carlo samples.

The $\tau^- \to \pi^- f_1 \nu_\tau$ branching fraction, using the $f_1 \to 2\pi^+2\pi^-$ decays, is measured to be

$$\mathcal{B}(\tau^- \to \pi^- f_1 \nu_\tau) = (4.73 \pm 0.28 \pm 0.45) \times 10^{-4}.$$

The result is obtained using $\mathcal{B}(f_1 \to 2\pi^+2\pi^-) = (11.0^{+0.7}_{-0.6})\times 10^{-2}$ [17].

The product of the $\tau^- \to \pi^- f_1 \nu_\tau$ and $f_1 \to \pi^+\pi^-\eta$ branching fractions is measured to be

$$\mathcal{B}(\tau^- \to \pi^- f_1 \nu_\tau)\mathcal{B}(f_1 \to \pi^+\pi^-\eta) = (1.26 \pm 0.06 \pm 0.06) \times 10^{-4},$$

based on a weighted average of the branching fractions of the three η modes. The $\mathcal{B}(\tau^- \to \pi^- f_1 \nu_\tau)$ branching fraction is determined to be $(3.59 \pm 0.19 \pm 0.35) \times 10^{-4}$ after dividing the product of the branching fractions by $\mathcal{B}(f_1 \to \pi^+\pi^-\eta) = 0.35 \pm 0.03$ [17]. We note that the Particle Data Group uncertainty on $\mathcal{B}(f_1 \to \pi^+\pi^-\eta)$ decreased from 0.11 to 0.03 in the 2011 partial update due to a re-evaluation of the existing data [17]. The significant difference in the $\tau^- \to \pi^- f_1 \nu_\tau$ branching fraction obtained using the $f_1 \to 2\pi^+2\pi^-$ and $f_1 \to \pi^+\pi^-\eta$ modes suggests that the $f_1 \to \pi^+\pi^-\eta$ branching fraction is too large. As a result we measure $\mathcal{B}(f_1 \to \pi^+\pi^-\eta)$ using

$$\begin{aligned}\mathcal{B}(f_1 \to \pi^-\pi^+\eta) &= \frac{[\mathcal{B}(\tau^- \to \pi^- f_1 \nu_\tau)\mathcal{B}(f_1 \to \pi^-\pi^+\eta)]}{\mathcal{B}(\tau^- \to \pi^- f_1 \nu_\tau)} \\ &= 0.265 \pm 0.022 \pm 0.027\end{aligned}$$

where a number of the systematic uncertainties cancel in the ratio. The largest uncertainty in $\mathcal{B}(f_1 \to \pi^+\pi^-\eta)$ is due to the uncertainty in the $f_1 \to 2\pi^+2\pi^-$ branching fraction [17] that is included in the $\tau^- \to \pi^- f_1 \nu_\tau$ branching fraction in the denominator.

The systematic uncertainties of the branching fractions are listed in Table II. We observe that the number of events in the f_1 peak in the $f_1 \to 2\pi^+2\pi^-$ sample varies by 5% for different background shapes. This variation is included as a systematic uncertainty. We also observe that the selection efficiency obtained from the Monte Carlo simulation has a slight dependence on whether the f_1 decays via the $f_1 \to a_0^- \pi^+$ or the $f_1 \to \pi^+\pi^-\eta$ mode, and the variation is included as a systematic uncertainty (listed under "Fit model" in Table II).

The $\tau^- \to \pi^- f_1 \nu_\tau$ branching fraction is consistent with the previous *BABAR* measurement [1]. CLEO published a branching fraction of $(5.8^{+1.4}_{-1.3} \pm 1.8) \times 10^{-4}$ [18] and Li predicts a branching fraction of 2.9×10^{-4} [19].

The f_1 mass is determined by fitting the peak with a non-relativistic Breit-Wigner function, which was used in previous measurements of the f_1 mass [17]. As a cross check, we fit the energy-momentum four-vectors from the generator Monte Carlo simulation and the peak value is found to be consistent with the input mass value.

We fit the invariant mass distribution in the fully-reconstructed Monte Carlo samples to determine whether it differs from the input mass of the Monte Carlo generator. The largest differences are observed in the modes with the highest number of neutral mesons in the final state (see Table III). The difference is used to correct the value of the invariant mass of each channel obtained from the fit and the uncertainty in the difference is included as a systematic error.

Table III and Fig. 3 show the results of the fits to the data. The last column of the table gives the mass after the application of the reconstruction correction factor. The average of these results is $M_{f_1} = (1.28025 \pm 0.00039)\,\mathrm{GeV}/c^2$.

Previous *BABAR* analyses have measured the invariant mass of resonances to be approximately $1\,\mathrm{MeV}/c^2$ less than the PDG value. This shift was observed in the measurement of the mass of the f_1 meson [20] and the τ lepton [21]. The shift has been attributed to the absolute energy and momentum calibration of the detector. We measure the calibration correction factor by fitting the η, ω, η', D^0 and D^{*-} states using data samples that have one track in the tag hemisphere and either three or five tracks in the signal hemisphere. No other selection criteria are applied. The invariant mass is found to be lower than the known values by (-0.91 ± 0.10) MeV/c^2 and the value is independent of mass of the resonance. The calibration correction factor is applied to the invariant mass and its error is included in the systematic uncertainty.

We determine the invariant mass of the $f_1(1258)$ meson to be

$$M_{f_1} = (1.28116 \pm 0.00039 \pm 0.00045)\,\mathrm{GeV}/c^2$$

The systematic uncertainty includes the reconstruction uncertainty and the calibration uncertainty. This result is in good agreement with the PDG value of (1.2818 ± 0.0006) GeV/c^2 [17].

C. $\tau^- \to (3\pi)^- \omega\nu_\tau$

We measure the $\tau^- \to \pi^-\pi^-\pi^+\omega\nu_\tau$ and $\tau^- \to \pi^-2\pi^0\omega\nu_\tau$ branching fractions. The number of events is determined by fitting the ω peak in the $\pi^+\pi^-\pi^0$ invariant mass distributions (see Fig. 4) with a Breit-Wigner distribution (the width of the ω is fixed to its nominal value), which is convolved with a Gaussian distribution to take into account the detector resolution. The resolution parameter of the Gaussian distribution is determined using a data control sample consisting of $q\overline{q}$ events, which is then fixed in the fit used to determine the branching fraction. A polynomial function is used to fit the background. The results are presented in Table IV.

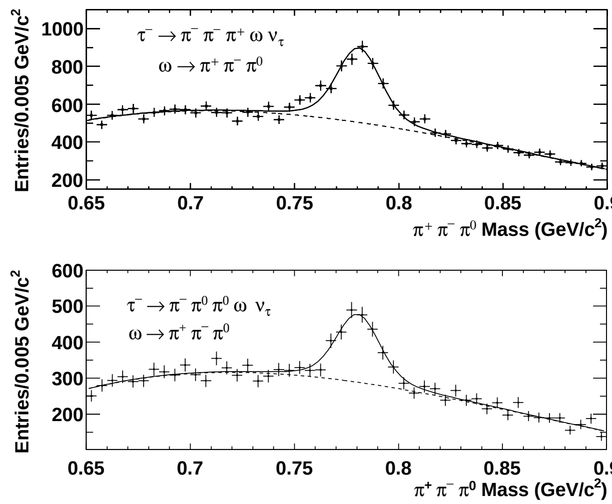

FIG. 4: The fits to the ω peak in the $\pi^+\pi^-\pi^0$ invariant mass distributions for $\tau^- \to \pi^-\pi^-\pi^+\omega\nu_\tau$ and $\tau^- \to \pi^-2\pi^0\omega\nu_\tau$ decays in the data sample after all selection criteria are applied. The solid lines represent the simultaneous fit to the ω peak and background. The dashed lines show the background function under the ω peak.

Approximately 10% of the events in the $\tau^- \to \pi^-\pi^-\pi^+\omega\nu_\tau$ channel are from backgrounds from other tau decays (primarily $\tau^- \to \pi^-\pi^0\omega\nu_\tau$ decays) and $e^+e^- \to q\overline{q}$ events.

The $\tau^- \to \pi^-2\pi^0\omega\nu_\tau$ sample has substantial contributions from $\tau^- \to \pi^-\omega\nu_\tau$ and $\tau^- \to \pi^-\pi^0\omega\nu_\tau$ decays. The background is estimated with the Monte Carlo simulation and verified using data and simulation control samples. The control samples follow the nominal selection criteria but select one or two π^0 instead of three π^0 mesons.

The branching fractions are found to be

$$\mathcal{B}(\tau^- \to \pi^-\pi^-\pi^+\omega\nu_\tau) = (8.4 \pm 0.4 \pm 0.6) \times 10^{-5}$$
$$\mathcal{B}(\tau^- \to \pi^-2\pi^0\omega\nu_\tau) = (7.3 \pm 1.2 \pm 1.0) \times 10^{-5}.$$

The systematic uncertainties are listed in Table IV. The uncertainty on the $\tau^- \to \pi^-2\pi^0\omega\nu_\tau$ branching fraction is dominated by the large contribution of the background decays.

The $\tau^- \to \pi^-\pi^-\pi^+\omega\nu_\tau$ and $\tau^- \to \pi^-2\pi^0\omega\nu_\tau$ branching fractions agree with the results from CLEO of $(1.2 \pm 0.2 \pm 0.1) \times 10^{-4}$ and $(1.4 \pm 0.4 \pm 0.3) \times 10^{-4}$, respectively [14]. Gao and Li suggest that this mode is dominated by the $(\pi\rho\,\omega)$ state and predict a branching fraction in the range of $1.8 - 2.1 \times 10^{-4}$ with the two modes ($\tau^- \to \pi^-\pi^-\pi^+\omega\nu_\tau$ and $\tau^- \to \pi^-2\pi^0\omega\nu_\tau$) having the same value [22]. The result measured in this work is ap-

TABLE III: Results of fits for the mass of the f_1 resonance in $\tau^- \to \pi^- f_1 \nu_\tau$ decays

Decay Mode	Monte Carlo (generator - fit) (GeV/c^2)	Data (fit) (GeV/c^2)	Data (corrected) (GeV/c^2)
$f_1 \to 2\pi^+ 2\pi^-$	0.00074 ± 0.00008	1.28031 ± 0.00067	1.28105 ± 0.00067
$f_1 \to \pi^+\pi^-\eta$			
$\eta \to \gamma\gamma$	0.00292 ± 0.00040	1.27775 ± 0.00045	1.28067 ± 0.00060
$\eta \to \pi^+\pi^-\pi^0$	0.00018 ± 0.00020	1.27787 ± 0.00080	1.27805 ± 0.00082
$\eta \to 3\pi^0$	0.00347 ± 0.00033	1.28036 ± 0.00335	1.28383 ± 0.00337

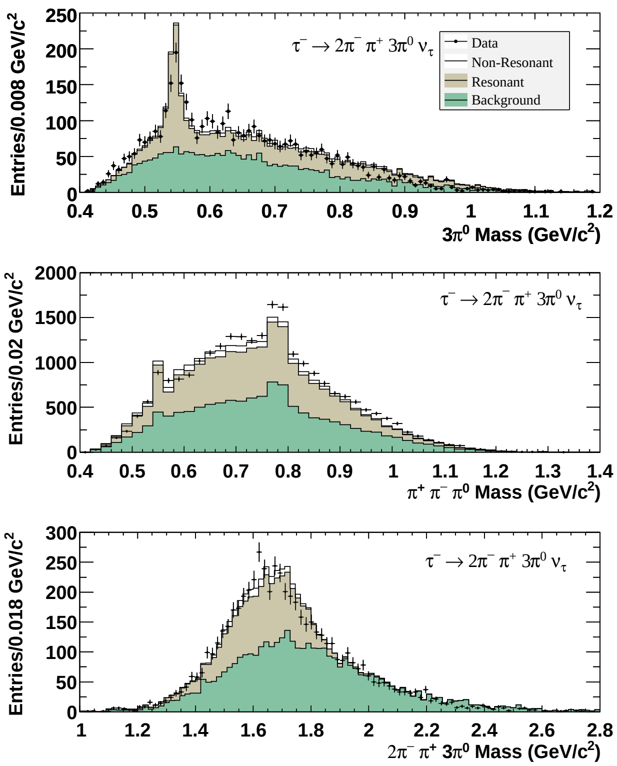

FIG. 5: The $3\pi^0$, $\pi^+\pi^-\pi^0$ and $\pi^-\pi^-\pi^+3\pi^0$ invariant mass distributions in $\tau^- \to \pi^-\pi^-\pi^+3\pi^0\nu_\tau$ decays. The prediction of the Monte Carlo simulation are shown for the resonant and non-resonant τ decays, and the background from other τ decays and $q\overline{q}$ events. The resonant decays include decays with correct topology and a resonance (η, f_1 or ω) in the final state. The contribution of the non-resonant decays is very small for this mode.

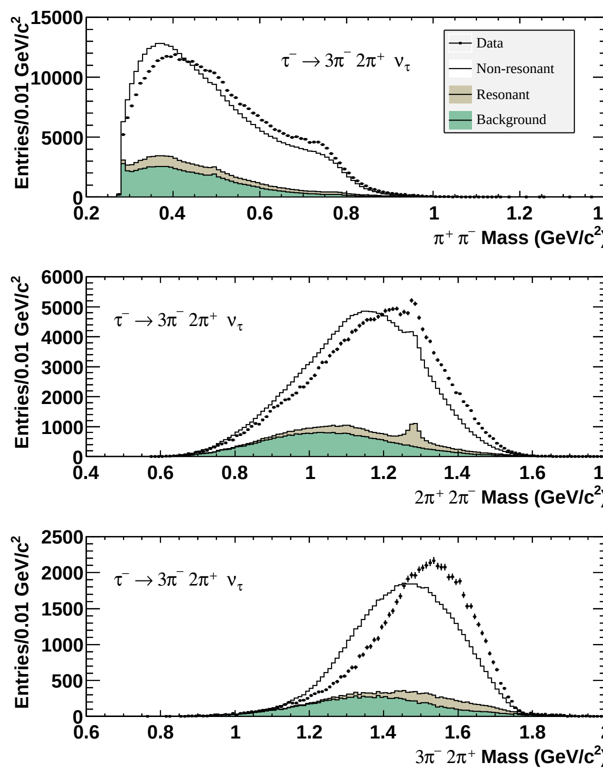

FIG. 6: The $\pi^+\pi^-$, $2\pi^+2\pi^-$ and $3\pi^-2\pi^+$ invariant mass distributions in $\tau^- \to 3\pi^-2\pi^+\nu_\tau$ decays. The prediction of the Monte Carlo simulation are shown for the resonant and non-resonant τ decays, and the background from other τ decays and $q\overline{q}$ events. The resonant decays include decays with correct topology and a resonance (η, f_1 or ω) in the final state. The non-resonant decays are generated using $\tau^- \to a_1^-\nu_\tau$. The difference between the data and Monte Carlo prediction is discussed in the text.

proximately 50% of the predicted rate but the ratio of the two branching fractions is consistent with unity.

D. Non-resonant decay modes

The resonant modes, involving η, ω and f_1 mesons, do not account for all of the observed decays. We consider the excess in the observed decays to be from "non-resonant" modes. We made no attempt to identify the contribution of resonances with broader widths ($> 100\,\mathrm{MeV}/c^2$) as the nature of these resonances is complex and their lineshape will be modified by the limited phase space in the τ decay. The Monte Carlo simula-

TABLE IV: Results and branching fractions of $\tau^- \to (3\pi)^- \omega \nu_\tau$ decays

	$\tau^- \to \pi^-\pi^-\pi^+\omega\nu_\tau$ $\omega \to \pi^-\pi^+\pi^0$	$\tau^- \to \pi^- 2\pi^0 \omega\nu_\tau$ $\omega \to \pi^-\pi^+\pi^0$
Branching fractions (10^{-4})	$0.84 \pm 0.04 \pm 0.06$	$0.73 \pm 0.12 \pm 0.10$
Data events	2372 ± 94	1135 ± 70
χ^2/NDF	55/44	42/44
Selection efficiency	$(3.27 \pm 0.03)\%$	$(0.75 \pm 0.01)\%$
Background	257 ± 71	709 ± 59
Systematic uncertainties (%)		
Tracking efficiency	3.8	2.7
π^0 and η PID	3.0	9.0
Pion PID	2.5	1.5
Lepton-tag PID	1.6	1.6
$\mathcal{L}\ \sigma_{\tau^+\tau^-}$	1.0	1.0
Selection efficiency	0.8	1.8
Background modeling	3.4	14
$\mathcal{B}(\omega \to \pi^-\pi^+\pi^0)$	0.8	0.8
Total (%)	6.8	17

TABLE V: Results and branching fractions of $\tau^- \to \pi^-\pi^-\pi^+3\pi^0\nu_\tau$, $\tau^- \to 3\pi^-2\pi^+\nu_\tau$ and $\tau^- \to 3\pi^-2\pi^+\pi^0\nu_\tau$ non-resonant decays

	$\tau^- \to \pi^-\pi^-\pi^+3\pi^0\nu_\tau$	$\tau^- \to 3\pi^-2\pi^+\nu_\tau$	$\tau^- \to 3\pi^-2\pi^+\pi^0\nu_\tau$
Branching fractions (10^{-4})	$0.06 \pm 0.08 \pm 0.30$	$7.68 \pm 0.04 \pm 0.40$	$0.36 \pm 0.03 \pm 0.09$
Data events	4094 ± 64	68985 ± 263	7296 ± 85
Efficiency	$(0.88 \pm 0.01)\%$	$(7.98 \pm 0.02)\%$	$(3.71 \pm 0.03)\%$
Background			
Resonant	1795 ± 221	4441 ± 370	4458 ± 244
Other τ decays	1681 ± 44	10621 ± 719	1315 ± 100
$q\overline{q}$	573 ± 50	1171 ± 205	359 ± 37
Total	4050 ± 231	16233 ± 835	6132 ± 267
Systematic uncertainties (%)			
Tracking efficiency	2	3.8	3.8
π^0 and η PID	9	-	3.0
Pion PID	1	2.5	2.5
Lepton-tag PID	2	1.6	1.6
$\mathcal{L}\ \sigma_{\tau^+\tau^-}$	1	1.0	1.0
Selection efficiency	2	0.2	0.9
Background modeling	520	1.6	22.9
Total (%)	520	5.2	23.7

tion models the final states using a phase space model for the final state particles. The only exception is the $\tau^- \to 3\pi^-2\pi^+\nu_\tau$ decay where Tauola models the decay using $\tau^- \to a_1^-\nu_\tau$ [23].

We measure the branching fractions of the non-resonant $\tau^- \to \pi^-\pi^-\pi^+3\pi^0\nu_\tau$, $\tau^- \to 3\pi^-2\pi^+\nu_\tau$ and $\tau^- \to 3\pi^-2\pi^+\pi^0\nu_\tau$ decays. The number of events is determined by subtracting the resonant decays and background from other τ decays and $q\overline{q}$ events from the total number of decays (see Table V).

The invariant mass plots in Fig. 5 show that the resonant decays dominate the $\tau^- \to \pi^-\pi^-\pi^+3\pi^0\nu_\tau$ mode.

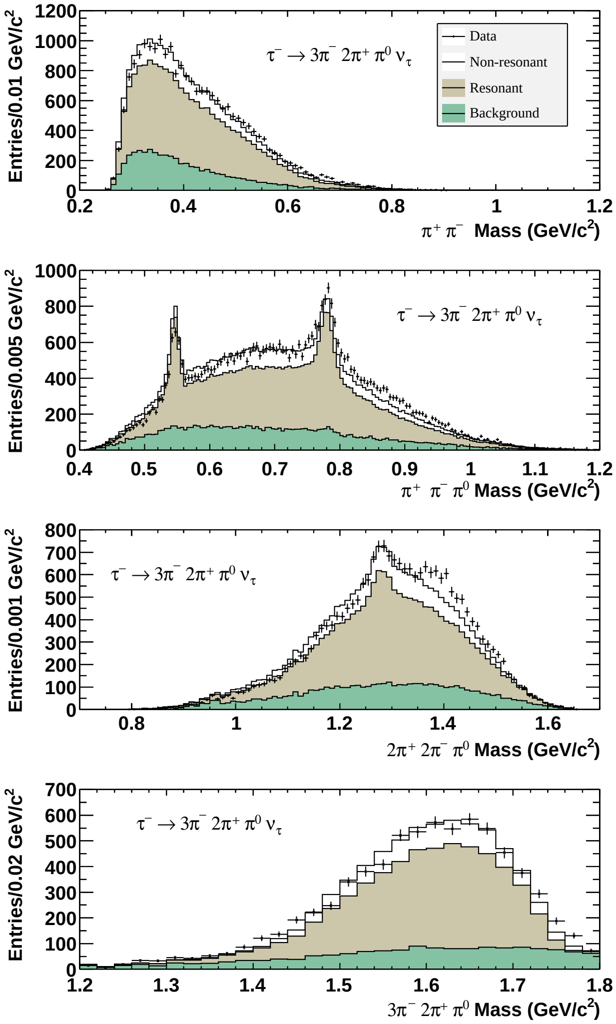

FIG. 7: The $\pi^+\pi^-\pi^0$ and $3\pi^-2\pi^+\pi^0$ invariant mass distributions in $\tau^- \to 3\pi^-2\pi^+\pi^0\nu_\tau$ decays. The prediction of the Monte Carlo simulation are shown for the resonant and non-resonant τ decays, and the background from other τ decays and $q\overline{q}$ events. The resonant decays include decays with correct topology and a resonance (η, f_1 or ω) in the final state. The resonant decays can account for a large fraction of this mode.

The background is primarily from $\tau^- \to \pi^-\pi^0\omega\nu_\tau$ and $q\overline{q}$ events. The branching fraction of the non-resonant $\tau^- \to \pi^-\pi^-\pi^+3\pi^0\nu_\tau$ is determined to be $(0.6\pm0.8\pm3.0)\times10^{-5}$ where the first error is statistical and the second systematic. The systematic uncertainty on the branching fraction is dominated by the uncertainty in the background which includes the Monte Carlo statistical uncertainty and the τ branching fraction uncertainties. The branching fraction is consistent with zero and we set a limit of

$$\mathcal{B}(\tau^- \to \pi^-\pi^-\pi^+3\pi^0\nu_\tau) \ < 5.5\times10^{-5}$$

at the 90% confidence level.

The $\tau^- \to 3\pi^-2\pi^+\nu_\tau$ decay, in contrast to the other two modes, has only a small contribution from resonant decays (see Fig. 6). The branching fraction of the non-resonant $\tau^- \to 3\pi^-2\pi^+\nu_\tau$ decay is determined to be

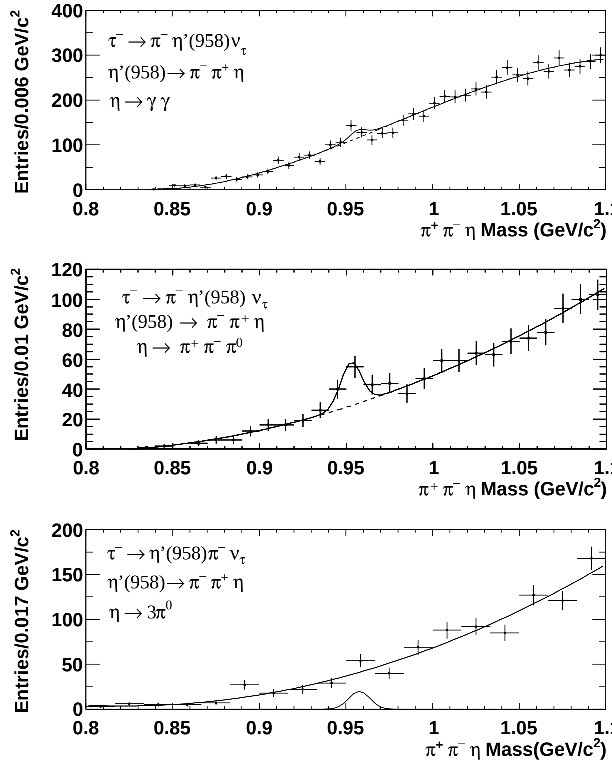

FIG. 8: The $\pi^+\pi^-\eta$ invariant mass in $\tau^- \to \pi^-\pi^-\pi^+\eta\nu_\tau$ decays for the $\eta\to\gamma\gamma$, $\eta\to\pi^+\pi^-\pi^0$ and $\eta\to3\pi^0$ decay modes in the data sample after all selection criteria are applied. The fit to the η' peak (in the top two plots) is represented by the solid line. The solid line in the bottom plot excludes the data point near the η' peak. The peak in this plot indicates the expected location and width of an η' signal.

$$\mathcal{B}(\tau^- \to 3\pi^-2\pi^+\nu_\tau) \ = (7.68\pm0.04\pm0.40)\times10^{-4}.$$

The $\tau^- \to \pi^-\pi^-\pi^+\omega\nu_\tau$ ($\omega \to \pi^-\pi^+\gamma$) is considered as a resonant background and is not included in the non-resonant branching fraction. Although the modeling of the $3\pi^-2\pi^+$ invariant mass distribution is not ideal, the selection efficiency remains the same if the Monte Carlo is re-weighted to resemble the data distribution. The decay model is a significant improvement over a phase space model (in which the ρ meson, observed in the $\pi^+\pi^-$ invariant mass distribution, would not be included) and further tuning of the model is required. The background of the $q\overline{q}$ events was checked by comparing the number of data and Monte Carlo events in the region above the τ lepton mass ($M > 1.8\,\mathrm{GeV}/c^2$). The branching fraction of the $\tau^- \to 3h^-2h^+\nu_\tau$ decay (where h is either a π^- or K^-) was measured to be $(8.56\pm0.05\pm0.42)\times10^{-4}$ in a previous *BABAR* publication [2] using a smaller data sample, which used no charged particle identification and the branching fraction included the contribution of the $\tau^- \to \pi^-\pi^-\pi^+\omega\nu_\tau$ decay.

The $\tau^- \to 3\pi^-2\pi^+\pi^0\nu_\tau$ decays are dominated by the resonant modes (see Fig. 7) and the branching fraction of the non-resonant $\tau^- \to 3\pi^-2\pi^+\pi^0\nu_\tau$ decay mode is

$$\mathcal{B}(\tau^- \to 3\pi^-2\pi^+\pi^0\nu_\tau) \;= (3.6 \pm 0.3 \pm 0.9) \times 10^{-5}.$$

There is an excess of data in the $2\pi^+2\pi^-\pi^0$ invariant mass distribution near $1.4\,\mathrm{GeV}/c^2$, which can be attributed to the $\tau^- \to \pi^-\omega'(1420)\nu_\tau$ ($\omega'(1420) \to \pi^+\pi^-\omega$), observed by *BABAR* in radiative return events [20]. The systematic uncertainty on the non-resonant $\tau^- \to 3\pi^-2\pi^+\pi^0\nu_\tau$ branching fraction is dominated by the large uncertainty in the background (see Table V). Although the invariant mass distributions of the resonant modes in the Monte Carlo simulation were corrected to give better agreement with the data, the corrections made little difference to the final branching fraction. The other τ decays and the $q\overline{q}$ events contribute to a lesser extent; their contribution to the uncertainty of the background is very small.

The $\tau^- \to 3\pi^-2\pi^+\pi^0\nu_\tau$ (including ω and excluding η) branching fraction is $(1.11 \pm 0.04 \pm 0.09) \times 10^{-4}$. This branching fraction can be compared with isospin model predictions [24, 25]. There are three τ decay modes with six pions in the final state: $\tau^- \to \pi^-\pi^-\pi^+3\pi^0\nu_\tau$, $\tau^- \to 3\pi^-2\pi^+\pi^0\nu_\tau$ and $\tau^- \to \pi^-5\pi^0\nu_\tau$ (there are no measurements of the $\tau^- \to \pi^-5\pi^0\nu_\tau$ decay mode). There are four possible isospin states for six pion decays: $(4\pi\rho)$, (3ρ), $(3\pi\omega)$ and $(\pi\rho\omega)$. The relative rate of the decays can be used to identify the dominant isospin states. The approximate equality of the $\tau^- \to \pi^-\pi^-\pi^+3\pi^0\nu_\tau$ and $\tau^- \to 3\pi^-2\pi^+\pi^0\nu_\tau$ branching fractions suggest that the $(4\pi\rho)$ and $(\pi\rho\omega)$ should dominate. The limited phase space imposed by the τ mass suppresses the higher mass states and as a result we do not observe evidence of the ρ meson in these decays.

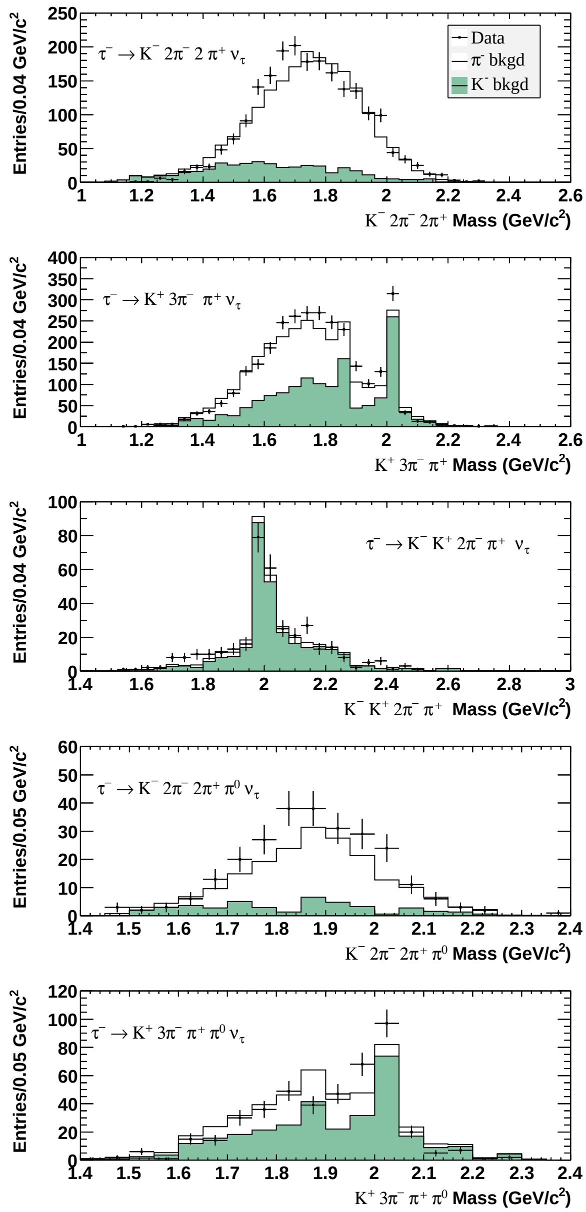

FIG. 9: The $K^-2\pi^-2\pi^+$, $K^+3\pi^-\pi^+$, $K^-K^+2\pi^-\pi^+$, $K^-2\pi^-2\pi^+\pi^0$ and $K^+3\pi^-\pi^+\pi^0$ invariant mass distributions in the data sample after all selection criteria are applied. The unshaded histogram represents τ decays in which a charged pion is mis-identified as a charged kaon, and the shaded histograms are primarily $q\overline{q}$ events in which there is a charged kaon in the final state. The Monte Carlo simulation does not include any signal decays.

E. Search for η' (958) decays

We next search for the $\tau^- \to \pi^-\eta'(958)\pi^0\nu_\tau$, $\tau^- \to K^-\eta'(958)\nu_\tau$ and $\tau^- \to \pi^-\eta'(958)\nu_\tau$ decays where $\eta' \to \pi^-\pi^+\eta$. The first two decays are allowed first-class decays whereas the last decay is a second-class decay with a rate that is expected to be zero in the limit of perfect isospin symmetry.

The selection efficiencies are determined using the signal Monte Carlo samples using the criteria described earlier. The numbers of signal candidates is determined by fitting the η' peak in the $\pi^+\pi^-\eta$ invariant mass distribution with a Gaussian function where the mean and resolution parameters are fixed to values obtained from a fit to η' mesons in a sample of $q\overline{q}$ events. In a number of cases (both $\tau^- \to K^-\eta'(958)\nu_\tau$ decays and the $\tau^- \to \pi^-\eta'(958)\pi^0\nu_\tau$ via $\eta' \to \pi^-\pi^+\eta$ and $\eta \to \pi^+\pi^-\pi^0$ decay) the statistics is too small for a fit and we count the number of events in the region around the η' mass and estimate the number of background events using the sidebands around the peak.

The $\pi^+\pi^-\eta$ invariant mass distribution for the $\tau^- \to \pi^-\eta'(958)\nu_\tau$ decays is shown in Fig. 8. The number of η' candidates is determined by the fit method for the $\eta \to \gamma\gamma$ and $\eta \to \pi^+\pi^-\pi^0$ channels and by the counting method for the $\eta \to 3\pi^0$ channel. We do not show the

TABLE VI: Results and branching fractions of $\tau^- \to \pi^-\eta'(958)\pi^0\nu_\tau$, $\tau^- \to K^-\eta'(958)\nu_\tau$ and $\tau^- \to \pi^-\eta'(958)\nu_\tau$ decays

$\tau^- \to \pi^-\eta'(958)\pi^0\nu_\tau$	$\eta \to \gamma\gamma$	$\eta \to \pi^+\pi^-\pi^0$	
Limit (90% C.L.)	1.4×10^{-5}	1.5×10^{-5}	
Branching fraction (10^{-6})	$7.8 \pm 4.1 \pm 1.7$	$0.0 \pm 0.7 \pm 0.9$	
Data events	24 ± 10	5 ± 6	
Background	5 ± 7	5 ± 8	
Selection efficiency	$(1.58 \pm 0.02)\%$	$(1.00 \pm 0.03)\%$	
$\tau^- \to K^-\eta'(958)\nu_\tau$	$\eta \to \gamma\gamma$	$\eta \to \pi^+\pi^-\pi^0$	
Limit (90% C.L.)	3.9×10^{-6}	4.2×10^{-6}	
Branching fraction (10^{-6})	$0.5 \pm 1.3 \pm 0.4$	$1.6 \pm 1.4 \pm 1.2$	
Data events	6 ± 7	15 ± 4	
Background	3 ± 4	11 ± 3	
Selection efficiency	$(3.47 \pm 0.03)\%$	$(3.09 \pm 0.04)\%$	
$\tau^- \to \pi^-\eta'(958)\nu_\tau$	$\eta \to \gamma\gamma$	$\eta \to \pi^+\pi^-\pi^0$	$\eta \to 3\pi^0$
Limit (90% C.L.)	5.7×10^{-6}	9.0×10^{-6}	2.1×10^{-5}
Branching fraction (10^{-6})	$-1.5 \pm 3.5 \pm 1.8$	$-0.4 \pm 3.9 \pm 4.3$	$10 \pm 6 \pm 5$
Data events	48 ± 22	44 ± 11	54 ± 7
Background	57 ± 11	45 ± 12	41 ± 6
Selection Efficiency	$(4.06 \pm 0.34)\%$	$(3.25 \pm 0.15)\%$	$(0.96 \pm 0.05)\%$

invariant mass distributions for the $\tau^- \to \pi^-\eta'(958)\pi^0\nu_\tau$ and $\tau^- \to K^-\eta'(958)\nu_\tau$ decays. The analysis of these decay modes uses only the $\eta \to \gamma\gamma$ and $\eta \to \pi^+\pi^-\pi^0$ channels (the $\eta \to 3\pi^0$ channel was not considered due to the limited size of the samples).

The results for the three decay modes are given in Table VI. The background from η' mesons is attributed to $e^+e^- \to q\overline{q}$ events and estimated using the Monte Carlo samples. The background estimation is validated by comparing the prediction of the Monte Carlo simulation with data for events where the invariant mass of all the observed final state particles is greater than the τ mass.

We find no evidence for $\tau^- \to \pi^-\eta'(958)\pi^0\nu_\tau$, $\tau^- \to K^-\eta'(958)\nu_\tau$ and $\tau^- \to \pi^-\eta'(958)\nu_\tau$ decays (see Table VI) and place upper limits on the branching fractions of

$$
\begin{aligned}
\mathcal{B}(\tau^- \to \pi^-\eta'(958)\pi^0\nu_\tau) &< 1.2 \times 10^{-5} \\
\mathcal{B}(\tau^- \to K^-\eta'(958)\nu_\tau) &< 2.4 \times 10^{-6} \\
\mathcal{B}(\tau^- \to \pi^-\eta'(958)\nu_\tau) &< 5.0 \times 10^{-6}
\end{aligned}
$$

at the 90% confidence level. The limits are determined from the average of the branching fractions measured for each mode. The $\tau^- \to \pi^-\eta'(958)\pi^0\nu_\tau$ and $\tau^- \to K^-\eta'(958)\nu_\tau$ are potential backgrounds to the $\tau^- \to \pi^-\eta'(958)\nu_\tau$ decay. We find that the background from these two decays is less than two events based on the upper limits on the branching fractions and we consider this background to be negligible. The previous limits on the $\tau^- \to \pi^-\eta'(958)\pi^0\nu_\tau$ were measured by *BABAR* to be 7.2×10^{-6} [1] and by CLEO to be 8×10^{-5} [18]. It is predicted that the branching fraction of $\tau^- \to \pi^-\eta'(958)\nu_\tau$ should be less than 1.4×10^{-6} [26].

F. Search for charged kaonic decays

Finally we present the first search for high-multiplicity τ decays with one or two charged kaons. We find no signal decays and place upper limits on the branching fractions of the $\tau^- \to K^-2\pi^-2\pi^+\nu_\tau$, $\tau^- \to K^+3\pi^-\pi^+\nu_\tau$, $\tau^- \to K^-K^+2\pi^-\pi^+\nu_\tau$, $\tau^- \to K^-2\pi^-2\pi^+\pi^0\nu_\tau$, $\tau^- \to K^+3\pi^-\pi^+\pi^0\nu_\tau$ and $\tau^- \to K^-\eta'(958)\nu_\tau$ decay modes (the $\tau^- \to K^-\eta'(958)\nu_\tau$ decay was presented in an earlier section).

The events are divided into topologies in which the charged kaon has either the same or opposite sign of the parent τ lepton. If there are two candidates, they must have opposite charge. All other tracks are required to be identified as charged pions. The selection criteria and systematic uncertainties have been described earlier. The requirement on the invariant mass ($M < 1.8\,\mathrm{GeV}/c^2$) of the final state uses the kaon mass for tracks identified as charged kaons (see Fig. 9). The prediction of the Monte Carlo simulation is divided into decays with K^- and decays without a K^- (in this case a π^- is mis-identified as a K^-). The figure does not include any signal decays in the Monte Carlo samples. The background estimate, which is the dominant systematic uncertainty, is verified by comparing the number of events in the data and Monte Carlo samples in the $M > 1.8\,\mathrm{GeV}/c^2$ region. If the kaon and τ have the same charge, then the background is from τ decays in which a π^- is mis-identified as a K^- meson.

The numbers of events selected in the data and Monte Carlo simulation are given in Table VII. The background predicted by the Monte Carlo simulation is approximately equal to the number of events in the data sample. There is an excess of data events in the $\tau^- \to K^-2\pi^-2\pi^+\pi^0\nu_\tau$ mode, but this excess extends to mass values above the τ mass, indicating that events are due to background τ decays or $q\overline{q}$ events.

The upper limits on the branching fractions are given in Table VII. There are no predictions for these modes. We estimate that $\mathcal{B}(\tau^- \to K^-2\pi^-2\pi^+\nu_\tau) \sim 10^{-5} - 10^{-6}$ if the decay is related to $\mathcal{B}(\tau^- \to 3\pi^-2\pi^+\nu_\tau)$ by the Cabibbo angle. The $\tau^- \to 3\pi^-2\pi^+\pi^0\nu_\tau$ decay is dominated by decays to the narrow low-lying resonances and the branching fraction of decay modes created by replacing a π^- with K^- would be highly suppressed due to the limited phase space.

IV. SUMMARY

We have presented measurements of the branching fractions of τ lepton decays to high multiplicity 3- and 5-prong final states. The results are shown in Table VIII (note that all modes are exclusive of the K^0_S meson). The results are more precise than previous measurements and many decay modes are studied for the first time.

Acknowledgments

We are grateful for the extraordinary contributions of our PEP-II colleagues in achieving the excellent luminosity and machine conditions that have made this work possible. The success of this project also relies critically on the expertise and dedication of the computing organizations that support *BABAR*. The collaborating institutions wish to thank SLAC for its support and the kind hospitality extended to them. This work is supported by the US Department of Energy and National Science Foundation, the Natural Sciences and Engineering Research Council (Canada), the Commissariat à l'Energie Atomique and Institut National de Physique Nucléaire et de Physique des Particules (France), the Bundesministerium für Bildung und Forschung and Deutsche Forschungsgemeinschaft (Germany), the Istituto Nazionale di Fisica Nucleare (Italy), the Foundation for Fundamental Research on Matter (The Netherlands), the Research Council of Norway, the Ministry of Education and Science of the Russian Federation, Ministerio de Ciencia e Innovación (Spain), and the Science and Technology Facilities Council (United Kingdom). Individuals have received support from the Marie-Curie IEF program (European Union) and the A. P. Sloan Foundation (USA).

[1] B. Aubert *et al.* (*BABAR* Collaboration), Phys. Rev. D **77**, 112002 (2008).
[2] B. Aubert *et al.* (*BABAR* Collaboration), Phys. Rev. D **72**, 072001 (2005).
[3] S. Banerjee, B. Pietrzyk, J.M. Roney and Z. Was, Phys. Rev. D **77**, 054012 (2008).
[4] B. Aubert *et al.* (*BABAR* Collaboration), Nucl. Instr. Methods Phys. Res., Sect. A **479**, 1 (2002).
[5] B. Aubert *et al.* (*BABAR* Collaboration), Phys. Rev. Lett. **99**, 021603 (2007).
[6] B. F. Ward, S. Jadach, and Z. Was, Comput. Phys. Commun. **130**, 260 (2000).
[7] S. Jadach, Z. Was, R. Decker, and J. H. Kühn, Comput. Phys. Commun. **76**, 361 (1993).
[8] T. Sjostrand, Comput. Phys. Commun. **82**, 74 (1994).
[9] E. Barberio and Z. Was, Comput. Phys. Commun. **79**, 291 (1994).
[10] D. J. Lange, Nucl. Instr. Methods Phys. Res., Sect. A **462**, 152 (2001).
[11] S. Agostinelli *et al.* (GEANT4 Collaboration), Nucl. Instr. Methods Phys. Res., Sect. A **599**, 250 (2003).
[12] S. Brandt *et al.*, Phys. Lett. **12**, 57 (1964); E. Farhi, Phys. Rev. Lett. **39**, 1587 (1977).
[13] The Novosibirsk function is defined as $f(m) = A\,\exp(-0.5\left\{\ln^2\left[1 + \Lambda\tau\cdot(m-m_0)\right]/\tau^2 + \tau^2\right\})$, where $\Lambda = \sinh(\tau\sqrt{\ln 4})/(\sigma\tau\sqrt{\ln 4})$, the peak position is m_0, the width is σ and τ is the tail parameter.
[14] A. Anastassov *et al.* (CLEO Collaboration), Phys. Rev. Lett. **86** 4467 (2001).
[15] B.A. Li. Phys. Rev. D **57** 1790 (1998).
[16] M. Acciarri *et al.* (L3 Collaboration), Phys. Lett. B **501**, 1 (2001).
[17] K. Nakamura *et al.* (Particle Data Group), J. Phys. **G37**, 075021 (2010) and 2011 partial update for the 2012 edition.
[18] T. Bergfeld *et al.* (CLEO Collaboration), Phys. Rev. Lett. **79** 2406 (1997).
[19] B.A. Li, Phys. Rev. D **55** 1436 (1997).
[20] B. Aubert *et al.* (*BABAR* Collaboration), Phys. Rev. D **76**, 092005 (2007).
[21] B. Aubert *et al.* (*BABAR* Collaboration), Phys. Rev. D **80** 092005 (2009).
[22] J. Gao and B.A. Li, Eur. Phys. Jour. C **22**, 283 (2001).
[23] J. H. Kuhn and Z. Was, Acta Phys. Polon. **B39** 147, (2008).
[24] A. Pais, Ann. Phys **9** 548 (1960).
[25] R.J. Sobie, Phys. Rev. D **60** 017301 (1999).
[26] S. Nussinov and A. Soffer, Phys. Rev. D **80**, 033010

TABLE VII: Results and branching fraction of charged kaon decay modes

	$\tau^- \to K^- 2\pi^- 2\pi^+ \nu_\tau$	$\tau^- \to K^+ 3\pi^- \pi^+ \nu_\tau$	$\tau^- \to K^- K^+ 2\pi^- \pi^+ \nu_\tau$
Limit (90% C.L.)	2.4×10^{-6}	2.8×10^{-6}	4.5×10^{-7}
Branching fraction (10^{-6})	$0.6 \pm 0.5 \pm 1.1$	$1.6 \pm 0.6 \pm 2.4$	$0.30 \pm 0.10 \pm 0.07$
Data events	1328 ± 36	1999 ± 45	32 ± 6
Background	1284 ± 72	1890 ± 163	15 ± 4
Selection Efficiency	$(7.9 \pm 0.1)\%$	$(7.9 \pm 0.1)\%$	$(6.7 \pm 0.1)\%$

	$\tau^- \to K^- 2\pi^- 2\pi^+ \pi^0 \nu_\tau$	$\tau^- \to K^+ 3\pi^- \pi^+ \pi^0 \nu_\tau$	
Limit (90% C.L.)	2×10^{-6}	8×10^{-7}	
Branching fraction (10^{-6})	$1.0 \pm 0.4 \pm 0.4$	$-0.6 \pm 0.5 \pm 0.7$	
Data events	112 ± 11	154 ± 12	
Background	87 ± 10	170 ± 16	
Selection Efficiency	$(2.9 \pm 0.1)\%$	$(2.9 \pm 0.1)\%$	

(2009).

TABLE VIII: Summary of branching fractions (excluding K_S^0)

Mode	Branching fraction
Resonant decays	
$\tau^- \to \pi^-\pi^-\pi^+\eta\nu_\tau$ (including f_1)	$(2.25 \pm 0.07 \pm 0.12) \times 10^{-4}$
$\tau^- \to \pi^-\pi^-\pi^+\eta\nu_\tau$ (excluding f_1)	$(1.00 \pm 0.09 \pm 0.13) \times 10^{-4}$
$\tau^- \to \pi^-2\pi^0\eta\nu_\tau$ (including f_1)	$(2.0 \pm 0.3 \pm 0.2) \times 10^{-4}$
$\tau^- \to \pi^- f_1\nu_\tau$	$(4.73 \pm 0.28 \pm 0.45) \times 10^{-4}$
$\tau^- \to \pi^- f_1\nu_\tau$ via $f_1 \to \pi^+\pi^-\eta$	$(1.26 \pm 0.06 \pm 0.06) \times 10^{-4}$
$f_1 \to 2\pi^+2\pi^-$	$0.265 \pm 0.022 \pm 0.027$
$\tau^- \to \pi^-\pi^-\pi^+\omega\nu_\tau$	$(8.4 \pm 0.4 \pm 0.6) \times 10^{-5}$
$\tau^- \to \pi^-2\pi^0\omega\nu_\tau$	$(7.3 \pm 1.2 \pm 1.0) \times 10^{-5}$
Non-resonant decays	
$\tau^- \to 3\pi^-2\pi^+\nu_\tau$ (excluding ω, f_1)	$(7.68 \pm 0.04 \pm 0.40) \times 10^{-4}$
$\tau^- \to \pi^-\pi^-\pi^+3\pi^0\nu_\tau$ (excluding η, ω, f_1)	$(0.6 \pm 0.8 \pm 3.0) \times 10^{-5}$
$\tau^- \to \pi^-\pi^-\pi^+3\pi^0\nu_\tau$ (excluding η, f_1)	$(16.9 \pm 0.8 \pm 4.3) \times 10^{-5}$
$\tau^- \to 3\pi^-2\pi^+\pi^0\nu_\tau$ (excluding η, ω, f_1)	$(3.6 \pm 0.3 \pm 0.9) \times 10^{-5}$
$\tau^- \to 3\pi^-2\pi^+\pi^0\nu_\tau$ (excluding η, f_1)	$(1.11 \pm 0.04 \pm 0.09) \times 10^{-4}$
Inclusive decays (including η, ω, f_1)	
$\tau^- \to \pi^-\pi^-\pi^+3\pi^0\nu_\tau$	$(2.03 \pm 0.18 \pm 0.37) \times 10^{-4}$
$\tau^- \to 3\pi^-2\pi^+\nu_\tau$ (excluding ω)	$(8.33 \pm 0.04 \pm 0.43) \times 10^{-4}$
$\tau^- \to 3\pi^-2\pi^+\pi^0\nu_\tau$	$(1.65 \pm 0.05 \pm 0.09) \times 10^{-4}$
η' (958) decays (90% upper level confidence limit)	
$\tau^- \to \pi^-\eta'(958)\pi^0\nu_\tau$	1.2×10^{-5}
$\tau^- \to K^-\eta'(958)\nu_\tau$	2.4×10^{-6}
$\tau^- \to \pi^-\eta'(958)\nu_\tau$	5.0×10^{-6}
Kaonic decays (90% upper level confidence limit)	
$\tau^- \to K^-2\pi^-2\pi^+\nu_\tau$	2.2×10^{-6}
$\tau^- \to K^+3\pi^-\pi^+\nu_\tau$	2.8×10^{-6}
$\tau^- \to K^-K^+2\pi^-\pi^+\nu_\tau$	4.5×10^{-7}
$\tau^- \to K^-2\pi^-2\pi^+\pi^0\nu_\tau$	2×10^{-6}
$\tau^- \to K^+3\pi^-\pi^+\pi^0\nu_\tau$	8×10^{-7}